



Continental shelf morphology controlled by bottom currents, mud diapirism, and submarine slumping to the east of the Gaoping Canyon, off SW Taiwan

Yi-Ching Yeh¹ · Chung-Lin Tsai¹ · Shu-Kun Hsu^{1,2} · Hsiao-Shan Lin² · Kuan-Ting Chen¹ · Yen-Yu Cho² · Chin-Wei Liang²

Received: 18 August 2020 / Accepted: 2 December 2020 / Published online: 7 January 2021
© The Author(s), under exclusive licence to Springer-Verlag GmbH, DE part of Springer Nature 2021

Abstract

The Gaoping River-Gaoping Submarine Canyon (GPC) is one of the dispersal river systems in the world. Tens of tons of terrestrial sediments discharge per year at the mouth of the river, where gravity-driven flow can damage the telecommunication cable along the 260-km-long GPC; to the east of the GPC, the continental shelf has been eroded. To understand this geological phenomenon, high-resolution sparker seismic data around the continental shelf as well as parallel and across the GPC were collected. Deep-towed sub-bottom profiler (SBP) data and data from shipboard acoustic Doppler current profiler were also collected. Three major system tracts off southwest Taiwan were identified, based on which the coastline of the last glacial maximum was identified at approximately 138 m below the current sea level. Analysis of the deep-towed SBP profiles suggested sandy sediment overflows through breakages on the east bank of the GPC. A convergence of bottom currents with a speed of up to 1.5 m/s flowing southeastward has eroded the continental shelf intensively, forming the Xiaoliuchiu channel. Although a mud diapir is active to the east of the GPC and forms the Xiaoliuchiu islet, it has been eroded at the Xiaoliuchiu channel. The average erosion rate on the east bank of the GPC was estimated to be approximately 609 cm/ka in the past 8.2 ka; between the GPC and the Xiaoliuchiu islet, the continental shelf is wasted due to severe seabed slumping.

Introduction

A submarine canyon is a sediment conduit or pathway that can transport sediments from the continental shelf down to the ocean basin. Based on their origin and nature of the connection to the river system, submarine canyons can be classified into three types: type I—shelf incising, which are associated with the river system; type II—shelf incising; and type III—blind or headless (Harris and Whiteway 2011). Most of the canyons worldwide belong to types II and III, accounting for 97.39% of the 5849 canyons. The type I canyon accounts for only 2.62 %, most of which were developed at active margin rather than at the passive margin. In addition, most type I

canyons are separated from the river mouth by a section of the continental shelf. The Gaoping Submarine Canyon (GPC) is characterized as a type I canyon in the active continental margin (Fig. 1a), and the canyon head almost reaches the mouth of the Gaoping river (GPR) (i.e., only 1 km separating them). It allows river plume induced gravity-driven flow, and the corresponding suspension flow to be transported to the GPC directly. A 260-km-long tectonically controlled GPC is connected to the GPR, which can be divided into three sections: upper reach, middle reach, and lower reach (Yu et al. 2009; Chiang and Yu 2006, 2008, 2011; Fig. 1a). The upper reach is affected by mud diapir activities (Chen et al. 2014; Hsu et al. 2018), which shows meandering and forms U-shaped canyons due to slope failures from lateral erosion. The mud diapir-based Xiaoliuchiu islet (Sun and Liu 1993; Liu et al. 1997; Lacombe et al. 2004; Hsu et al. 2018) is placed at the junction of the canyon wall breakage and the river meandering southwestward (Fig. 1b). The middle reach of the GPC is dominated by thrusting fault deformation, revealing a linear and V-shaped down-cutting canyon. In the lower reach, the river reverts to meandering, forming a U-shaped canyon. According to statistics, up to 49 mega tons of

✉ Yi-Ching Yeh
yeyeh@ncu.edu.tw; yiching.yeh@gmail.com

¹ Department of Earth Sciences, National Central University, Jhongli 32001, Taiwan

² Center for Environmental Studies, National Central University, Jhongli 32001, Taiwan

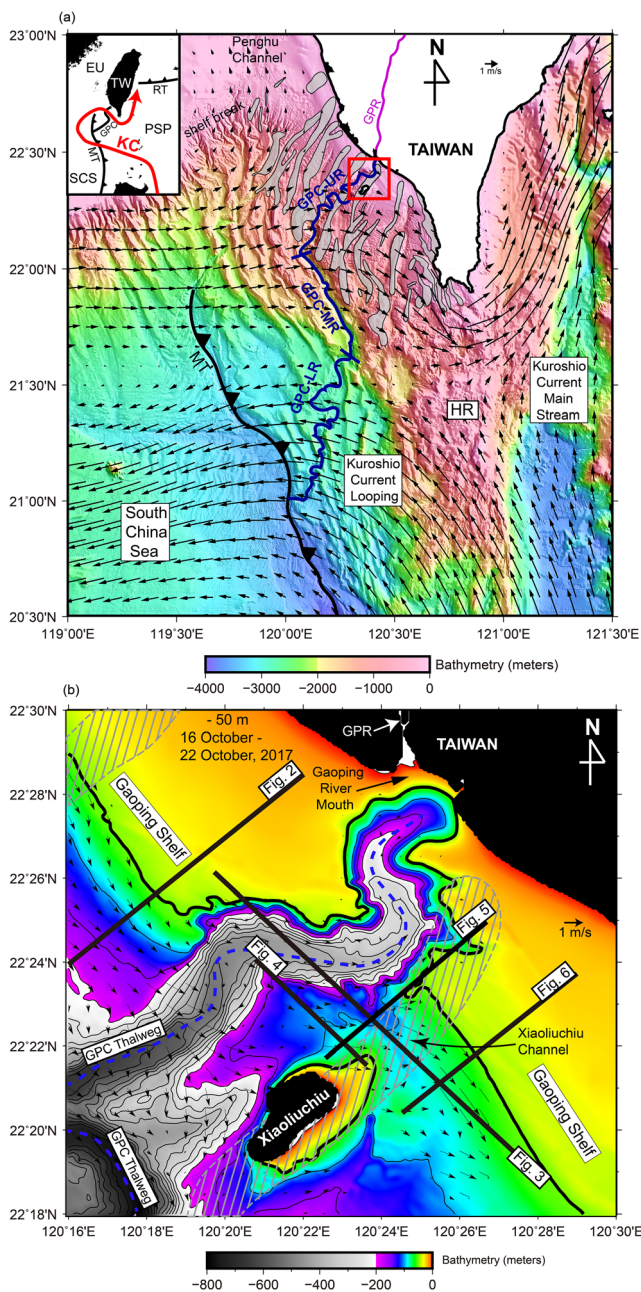


Fig. 1 (a) Tectonic framework and 27-year (1992–2019) monthly average of geostrophic current field from AVISO⁺ website (<http://www.aviso.oceanobs.com/en/data/>) imprinted on swath bathymetric data (Liu et al. 1998) in the southwestern offshore Taiwan. Bold blue lines mark segment boundaries of the Gaoping Submarine Canyon (GPC); (b) Swath bathymetric map of the study area. Thin black line with arrow represents ADCP horizontal composite current velocity field near the seafloor (50 mbsf) during Fall of year 2017 (i.e., ORI-1179 cruise). Black bold lines represent sparker seismic profiles (Figs. 2, 3, and 6) and deep-towed sub-bottom profiler profile sections (Figs. 4 and 5). Grey pattern and grey slash pattern: mud diapirs distribution (Chen et al. 2014); GPR, Gaoping River; GPC, Gaoping Canyon; GPC-UR, Gaoping Canyon upper reach; GPC-MR, Gaoping Canyon middle reach; GPC-LR, Gaoping Canyon lower reach; KC, Kuroshio Current looping; HR, Hengchun Ridge

terrestrial sediments per year (i.e., a quarter of the total sediment discharge in Taiwan) are discharged from the GPR,

which is the second largest river drainage system in Taiwan (Dadson et al. 2003). In the last decade, several studies have been conducted, with focus on the morphological features of the GPC and the surrounding area (Yu et al. 1993; Yu et al. 2009; Chiang and Yu 2006, 2008, 2011; Chiang et al. 2020), sediment dynamics and physical properties of the water column along the canyon (Liu et al. 2016), and surface sediment characteristics (Su et al. 2018). Some studies have focused on sedimentary structures of the deep-sea fan (i.e., Gaoping fan; Hsiung et al. 2018) and overbanking flow correlated with climate variation over the last 20,000 years in the lower reach of the canyon (Yu et al. 2017). However, the upper reach is the source that can generate gravity driven sediment flow and suspension flow, which has not been investigated and discussed in relation to near-seafloor sedimentary structures and dynamics (deposition or erosion) and its relationship with bottom current. This paper is presented an intense seafloor erosional structure produced by the bottom current that interacts with the mud diapir in the upper reach of the GPC, derived from sparker seismic and deep-towed sub-bottom profiler (SBP) data. Integrated analysis with acoustic Doppler current profiler (ADCP)—a dynamical sediment deposition and erosion model—is employed to explain the relationship between canyon overflow, erosion, and transportation in the upper reach of the GPC.

Physical setting

Gaoping Submarine Canyon sediment dynamics

Due to rapid uplift, heavy rainfall induced by annual typhoons, and the southwest monsoon in the study area, large amounts of terrestrial sediments are eroded and flushed down to the deep sea through the GPC (Dadson et al. 2003). In 2009, the typhoon Marokot caused strong rainfall, which triggered numerous landslides in southwest Taiwan. Sediments were discharged through the GPR and formed a turbidity current at the river mouth that flushed down the 260-km-long canyon and broke the submarine telecommunication cable along the pathway (Carter et al. 2012). In addition to river flooding, earthquakes can be one of the factors that trigger slope failures, inducing the turbidity current that damages the submarine cable (e.g., Pingtung earthquake in 2006; Hsu et al. 2008). The speed of the turbidity current is estimated from the time of cable break and can be up to approximately 20 m/s in the upper slope; this can destroy constructions along and across canyons, trigger slope failure along reworked sediment, and amplify the magnitude of the turbidity current. According to previous studies, the deeper portions of the GPC are dominated by the tidal current moving up the canyon during winter (Liu et al. 2016). In contrast, river plume sediments induce gravity-driven flow (e.g., hyperpycnal flow or gravity flow) at

the mouth of the Gaoping river, which moves downward along the canyon thalweg (Liu et al. 2016; Yu et al. 2017). This can erode the seafloor continuously and may produce overbanking sediments through canyon breakage, specifically in the upper and lower reaches of the GPC (Yu et al. 2017). The suspension plume and spread consist of relatively fine grained sediments that are deposited on both banks of the GPC (Liu et al. 2016). The piston/gravity sediment cores collected between 2005 and 2015 by *R/V Ocean Researcher* suggested that river plume suspension sediments were deposited on both banks of the GPC (Su et al. 2018). The grain size is coarser (i.g. median sand) on the east bank with more turbidity current deposits close to the seafloor (Su et al. 2018). This probably indicates the existence of canyon overbanking flow deposits on the east bank of the upper reach of the GPC. However, due to the low resolution of stratigraphic mapping near the seafloor, the sediment dynamics in the upper reach of the GPC are yet to be determined.

Kuroshio Current looping

The Kuroshio Current (KC) originates from the north equatorial current and flows offshore of east Luzon, Taiwan, and the Japanese islands. During summer, the main stream of the KC flows northward along the east of the western Pacific island chain.

Only a part of the water from the KC leaks through the Bashi Strait between Taiwan and Luzon. However, during winter, the KC can transgress westward to the northern South China Sea area through the Luzon Strait and loop clockwise between the northern South China Sea passive margin and southwestern offshore Taiwan. The looping KC may merge back with the main stream offshore of southeastern Taiwan through the Bashi Strait (Jan et al. 2002, 2010, 2019). Several studies that used the Atlas Buoy, ship board conductivity, temperature, and density (CTD) meter, and numerical modeling have suggested that the KC intrudes the northern South China Sea in three different ways: looping, leaking, and leaping (Nan et al. 2015; Yang et al. 2020). Looping can occur in any season, but the period from fall to winter has a higher probability of occurrence, exhibiting relatively steady and strong NW–SE trending flow in the continental margin offshore southwestern Taiwan (Nan et al. 2015; Yang et al. 2020). However, to date, there have been no reports on or discussions regarding the interaction between the looping KC and seafloor geological processes, such as sediment deposits (e.g., drift), erosion (e.g., furrow or channel), and migration (source to sink), particularly in the shelf to slope transition offshore of southwestern Taiwan. Figure 1a presents the bathymetry and tectonic setting offshore of southwestern Taiwan. The monthly averaged geostrophic current field between 1992 and 2018 obtained from the AVISO⁺ website at <http://www.aviso.oceanobs.com/en/data/> shows that the main

stream of the KC intrudes the northern South China Sea area and rotates clockwise. The KC looping causes NW–SE trending flows along the Gaoping continental slope. Figure 1b shows a detailed swath bathymetric map of the upper reach of the GPC area. The 50-m contour line is noted to be the boundary separating the shelf and slope. The continental shelf is approximately 10-km wide on the west bank of the GPC. Contrary to the west bank, the shelf shrinks 2-km landward in the east bank, and there is a clear NW–SE trending Xiaoliuchiu channel north of the Xiaoliuchiu islet. In addition, the seafloor relief reveals an average drop of 20 m (maximum of 40 m) on the east bank of the canyon with respect to the west bank. How can the Xiaoliuchiu channel develop in the continental shelf-to-slope transition area? How is a channel in the high sedimentation-rate area close to the river mouth and the relationship between current field, geological process, and corresponding sediment dynamics in the uppermost canyon area, maintained? This study aims to demonstrate high-resolution seismic profile structures since the last glacial maximum (LGM) and discusses the erosional process in the uppermost part of the GPC from the bottom current induced by the KC looping offshore of southwestern Taiwan.

Materials and methods

Although significant marine geophysical data have been collected offshore of southwestern Taiwan in the past decade, only data pertaining to conventional active deep penetration and of lower resolution (i.e., higher than 40 m) are available for the study area. This study aims to explore shallow high-resolution seismic profile structures and related sediment dynamics. To accomplish this task, two types of high-resolution marine geophysical exploration methods were applied in this study: the marine sparker reflection seismic method and the deep-towed sub-bottom profiler.

Sarker seismic data

The sparker uses electrode-electrode voltage to create spark pulses for an extremely short period (i.e., a few milliseconds) in seawater, capable of producing high-resolution wavelets of 30–800-Hz frequency range, which represents the seismic source. The interval between shots was set to 10 s, which is equivalent to approximately 20-m shot interval with respect to the ground, for an average ship speed of four knots. In the meantime, a 60-m-long fluid-type streamer with 48 hydrophones was deployed, composed of two active channels with a 0.125-m.s. sampling rate. To better illustrate the structural framework of the uppermost part of the GPC, 40 two-dimensional (500 m) spacing profiles (ORI-1179 cruise) across the GPC, from the GR mouth to Xiaoliuchiu islets, were collected. Furthermore, eight sparker seismic profiles

(ORI-1180 cruise) perpendicular to the topographic contour were collected as cross check lines. Owing to the instabilities of the sparker source, the source waveform is not in minima phase. Therefore, before further data processing, the application of a match filter is necessary to transform raw seismic records to a minima phase waveform. The data processing procedure is as follows. A 30-200-400-800-Hz zero-phase bandpass filter, which is an F–K filter, was used to eliminate random noise. For sound velocity in water of 1500 m/s, normal move-out correction and stack were applied followed by a post-stack spiking/predictive deconvolution with a 12-m.s. predictive length and 80-m.s. operator length. Finally, a 30-60-300-600-Hz minima phase bandpass filter, spherical divergence correction, and 100-m.s. window length automatic gain control (AGC) were applied. The processed profiles were plotted using free Seismic Unix 44R2 version software (Stockwell and Cohen 2002). In this study, one sparker seismic profile across the GPC was chosen to show differences in near-seafloor sedimentary structure between the western and eastern banks of the GPC (Fig. 1b). The other two profiles are across the Gaoping Slope, which shows seismic parasequences since the last glacial period (Fig. 1b).

Deep-towed sub-bottom profiler data

To better constrain near-seafloor fine sedimentary structures, Edgetech 2000 CSS deep-towed SBP was employed to collect data sub-parallel to high-resolution sparker seismic lines. To better image sub-seafloor stratigraphy across the Gaoping Canyon, towed fish height was set as 30–50 m depending on the water depth in the west and east bank of the canyon. Before any processing, the SBP data were laid back to its original position based on the GPS position of the research vessel and in situ bathymetry along the ship track. The raw SBP data were converted to conventional seismic segy format and then input to a commercial seismic data processing software (Paradigm EchosTM version 17) for further random noise attenuation and filtering; the data were then subject to time-variant gain and AGC for balancing the amplitude and output before plotting using Generic Mapping Tools version no. 5 (GMT; Wessel et al. 2013). In this study, two SBP sections were selected to demonstrate near-seafloor sedimentary structures (Fig. 1b).

Acoustic Doppler current profiler data

To constrain near-seafloor current field to the study area, data from shipboard ADCP from two cruises (ORI-1179 cruise between October 16 and October 22, 2017; ORIII-2019 cruise between August 30 and September 1, 2017) were used along the sparker seismic survey tracks. The CASCADE software version 7.2 (Le Bot et al. 2011) developed by LOPS (Laboratory for Ocean Physics and Satellite remote sensing)

was used to process the ADCP data. The data processing procedure included data import, bottom tracking, data cleaning, tidal correction, filtering, and data output. The output data in ASCII format is flagged from 1 to 8 based on data quality. In this study, only flag #1 (i.e., suitable data) was used for gridding and producing the current-field map.

Seismic interpretation

In this section, seismic interpretations of three sparker seismic profiles and two deep-towed SBP profiles are presented (Figs. 2, 3, 4, 5, and 6). For convenience, two-way travel time is converted to true depth by a sound velocity in water of 1500 m/s. Due to the lack of sediment corings for the study area, seismic data interpretations in this study are based on the principles of seismic stratigraphic analysis (Vail et al. 1977; Mitchum et al. 1977) and seismic parasequences analysis of the continental slope (Van Wagoner et al. 1988, 1990). Based on seismic amplitude, continuation, and termination, three major system tracts can be identified, from deep to shallow, in the study area: lowstand system tract (LST), transgressive system tract (TST), and highstand system tract (HST). In addition, to understand the interaction between the bottom current and near-seafloor sedimentary structures, sparker seismic data, deep-towed sub-bottom data, and data from shipboard ADCP were integrated for interpretation.

Figure 2 illustrates a sparker seismic profile perpendicular to the Gaoping Shelf on the west bank of the GPC. The depth of water along this profile varies from 200 (southwest end) to 30 m (northeast end), which includes the entire continental shelf domain and shelf break area. The seismic section shows a relatively smooth seafloor in the northeast end close to the Taiwan coast, becoming wavy with a clear gliding surface just beneath the seafloor, which may be interpreted as creeping sediment waves (i.e., Levchenko and Roslyakov 2010) (profile distance between 0.8 and 2.2 km). Below the sediment waves, seismic amplitude reveals irregular, disconnected, and strong-reflection stratigraphy aggregates seaward along the slope that may reflect suspension sediments from the GR plume (i.e., position 1–2 km in Fig. 2). A continuous and strong-amplitude dip interface delimitates the slope deposits. Below the interface, seismic characteristics change to horizontal and continuous reflection and onlap to slope, with strong reflection at the shelf break (see Fig. 2 position 0–3 km). Therefore, the dip interface can be identified as the parasequence boundary, which is the maximum flooding surface (MFS) that separates the HST above from the TST below. At the bottom of the TST, the seismic characteristic changes to a strong amplitude, continuous with the channel fills (see strong U-shaped reflections approximately 200 m below the sea surface (mbsf) in Fig. 2 closeup) that reflects a low sea level period (i.e., transgressive surface; TS). Below the TS

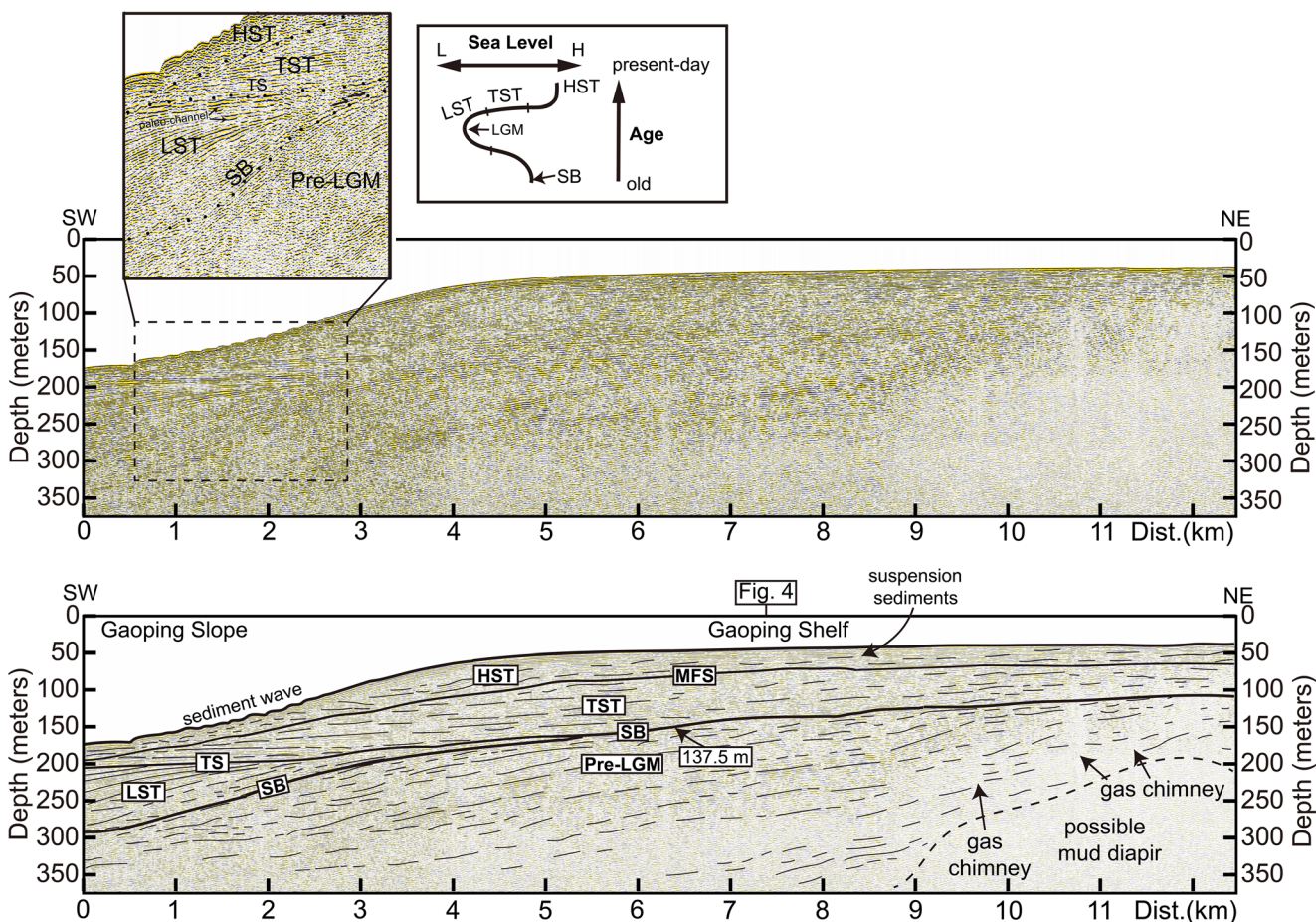


Fig. 2 Sparker seismic profile across the Gaoping Shelf on the west bank of Gaoping Canyon. Upper panel shows raw seismic profile. Lower panel shows raw seismic profile with interpretations. Black box is a close up showing seismic characteristics of each system tract near the shelf break

and corresponding sea level status since last glacial period: system tract boundary. HST, Highstand System Tract; TST, Transgressive System Tract; LST, Lowstand System Tract; MFS, Maximum Flooding Surface; SB, sequence boundary (paleo seafloor); TS, Transgressive Surface

interface, a westward convex sequence, with 250-m lateral interval, overlaps and propagates from a position of 3 km toward the west end of the profile. The clinofolds top lap horizontally onto the TS interface, and the entire clinofold is thinner landward and pinches out at a position of 5.2 km. This is a typical feature of the sea level during the lowstand period of deposits. Therefore, the LST is bounded by the paleo-seafloor (SB in Fig. 2) and TS (Fig. 2). Below the SB, this portion belongs to the paleo-seafloor and related sedimentary sequence. The sedimentary process evolution in the study area is shown in Fig. 2. In summary, the sea level started to fall, causing seafloor erosion and development of a sequence boundary (SB in Fig. 2 closeup). The sea level continued to fall, allowing terrestrial sediments to be transported to the paleo-shelf break (positions 5.2 km and 170 mbsf) and form numerous clinofolds, such as the LST. After the last glacial maximum (LGM), the sea level started to rise and formed the TST with horizontal and continuous strong amplitude sequence. The sea level then rose continuously and developed a MFS and corresponding HST stratigraphy. In summary,

TST thickness varies from 10 m at the current shelf break to 75 m at the paleo-shelf break (at approximately 5-km position). The HST thickness is nearly 25–30 m, which is thinner than the TST.

Figure 3 and Fig. 4 illustrate a sparker seismic section and corresponding deep-tow SBP section across the GPC in the vicinity of the Xiaoliuchi islet. On the west bank of the canyon, the paleo-seafloor (SB in Fig. 3) is identified at approximately 137.5 mbsf. The overlying TST and HST have the same thickness (i.e., 50 m) on the western bank of the GPC, and the near-seafloor stratigraphy is relatively horizontal and smooth, without erosional features. The sediment column was cut by approximately 8° with a southeast dip along the west wall of the GPC. The thalweg of the GPC is located at a position of 4.4 km and 425 mbsf, which shows a continuous and relatively flat surface with a strong amplitude. Below the seafloor, three major depositional cycles (i.e., position 4–6 km in Fig. 3) can be identified that exhibit similar seismic sequence characteristics, where seismic amplitude varies from high near the bottom of the sequence to low at the top. In

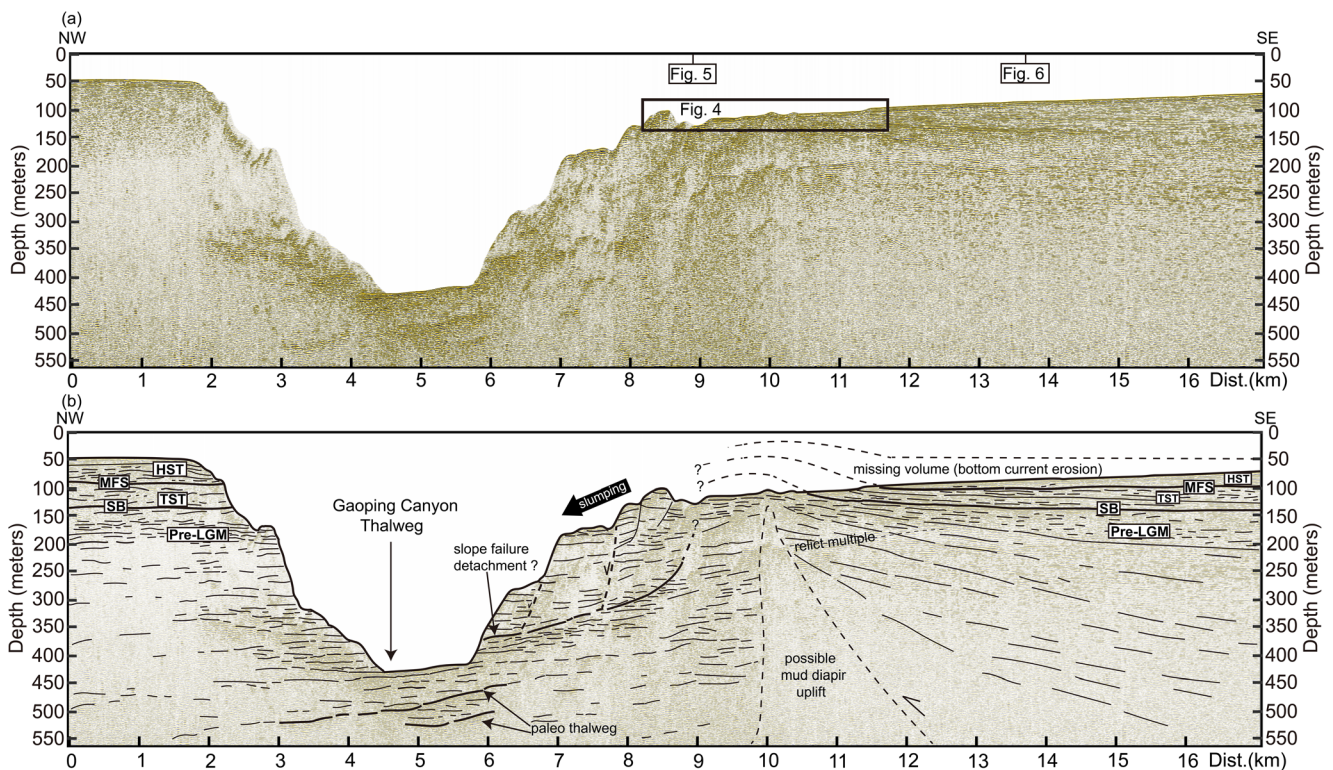


Fig. 3 Sparker seismic profile across GPC north of Xiaoliuchiu islet and its interpretations. The black square represents corresponding deep-towed sub-bottom profiler profile section. The dashed polygon indicates

possible eroded area by bottom current erosion. HST, Highstand System Tract; TST, Transgressive System Tract; MFS, Maximum Flooding Surface; SB, Sequence Boundary (paleo seafloor)

addition, these events are confined to a narrow 2-km-wide region that indicates only slight migration in the thalweg of this portion of the GPC. On the east bank of the canyon, a listric, strong amplitude seismic reflector with continuous interface cuts from the east bank of the seafloor (position 9 km in Fig. 2) and diminishes at the east canyon wall (position 5.8 km in Fig. 2). The stratigraphy above the listric surface shows block rotation that is stepped down northwest toward the canyon, which is a typical feature of slope failure. In the east vicinity of the slope failure, an asymmetrically tilted stratigraphy bounded by a cone shape structure with chaotic to blank reflection intrudes and disturbs near-seafloor stratigraphy (approximately 125 mbsf). This probably indicates mud diapir uplift and corresponding slope failure, which was also reported in the Gaoping Slope area (Chen et al. 2018). East of

the mud diapir, all sequences are tilted toward the top of the mud diapir, the HST sequences are fully whiped out, and only the TST is outcropped (position 9–11.8 km). Most erosion occurred between positions 8.6 and 10.5 km, both TST and HST were peeled off, and stratigraphy prior to the LGM is exposed on the seafloor. Since asymmetrical uplift in position 9–13 km in Fig. 3, this uplift could be interpreted as interaction between thrusting fault and mud diapirism (position 11–13 km in Fig. 3). At the east of position 11.8 km, the HST has a wedge shape and the thickness increases up to 25 m, which is only half of the HST thickness on the west bank of the GPC. This indicates that the east bank of the GPC belongs to an erosional environment. In addition, an SBP section (Fig. 4) shows numerous truncated high-amplitude eastward propagation sequences down-lapping on a relatively flat interface,

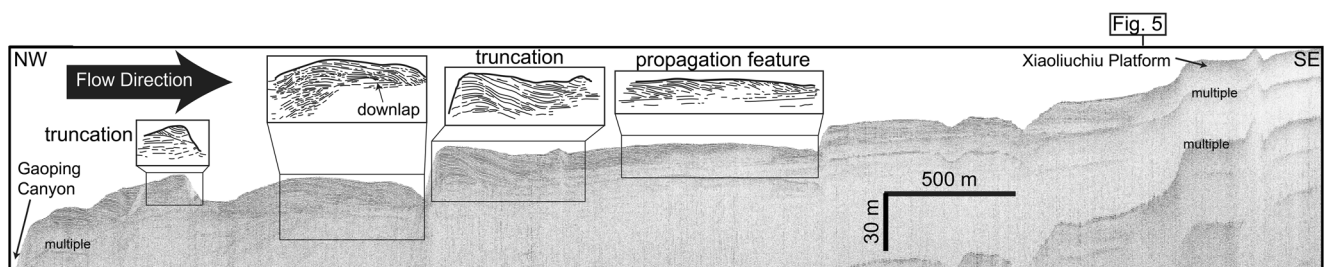


Fig. 4 Deep towed sub-bottom profiler image across GPC north of Xiaoliuchiu islet. Noted that high reflective amplitude strata down-lap and propagates from GPC to Xiaoliuchiu platform. There is clear seismic truncation on the seafloor

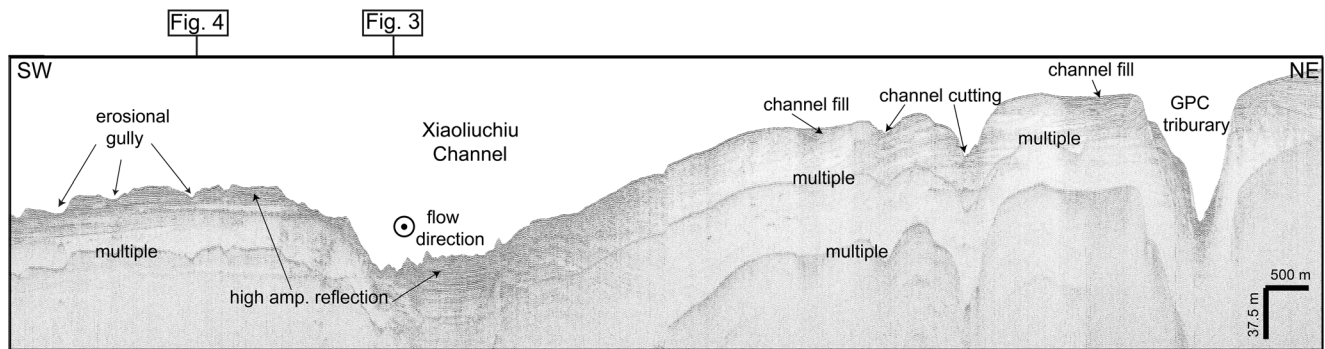


Fig. 5 Deep towed sub-bottom profiler image adjacent to east wall of GPC. Noted that sub seafloor high reflective amplitude strata are accompanied by series of erosional gullies and channels in the Xiaoliuchi channel

which suggests sediments of turbidity origin transported from the GPC toward the Xiaoliuchi platform (Fig. 3a). Furthermore, the profiles collected from the ship board ADCP in October, 2017 and July, 2018 (Figs. 1b, S1, S2, and S3) suggest strong bottom current (up to 1.5 m/s) surges down to the seafloor, which can explain the erosional mechanism on the east bank of the GPC. Combined with results from SBP sections, sparker seismic sections, and data from the ship board ADCP, it is inferred that the mud diapir adjacent to the east wall of the GPC uplifts and induces slope failure; the bottom current induced by the NW–SE trending KC looping eroded both TST and HST sequences on top of the mud diapir.

Figure 5 and Fig. 6 demonstrate the deep-towed SBP and the corresponding sparker seismic profile sections on the east bank of the GPC. In Fig. 5, a SBP section close to the east wall of the GPC shows a relatively high reflective amplitude strata near the seafloor, adjacent to the Xiaoliuchi channel, which probably indicates overbank flow deposits. The north of the Xiaoliuchi channel exhibits low reflective amplitude near the seafloor strata, which suggests finer grain deposits. In

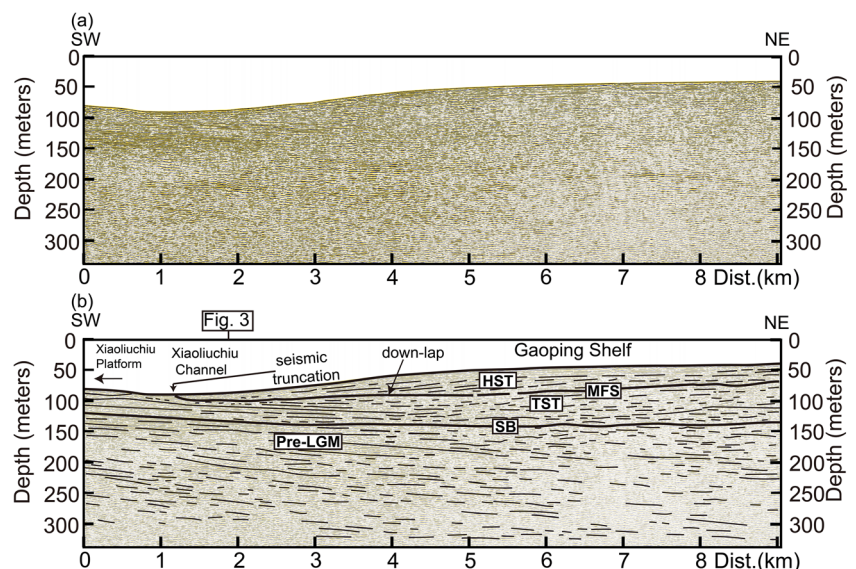
contrast, existence of down-cutting gullies and truncated strata suggests tremendous seafloor erosion in the Xiaoliuchi channel. Based on seismic stratigraphic analysis of the sparker seismic section (Fig. 6), it is observed that HST sediments were eroded fully with thin transgressive system tract sediments (approximately 10-m thick), which indicates that erosion has been occurring for a long period since the LGM period.

Discussion

Xiaoliuchi channel: relict channel or in situ erosional channel?

The Xiaoliuchi channel is located in the northernmost area of the GPC with a water depth of less than 100 m (see Fig. 1). In addition, Lambeck et al. (2014) suggest that the sea level was 120 m below the present-day sea surface during the LGM period, exposing the Gaoping shelf area. This could probably

Fig. 6 Sparker seismic profile perpendicular to Gaoping slope strike and its interpretations for the east bank of the GPC. (a) Raw sparker seismic profile; (b) Sparker seismic profile with interpretations. A considerably thin TST and an absent HST are observed in the V-shaped topographic depression that suggests existence of a strong and long-term erosional event. HST, Highstand System Tract; TST, Transgressive System Tract; SB, Sequence Boundary (paleo seafloor); MFS, Maximum Flooding Surface



have led to the development of channels or tributaries of the GPC. However, the uppermost part of the GPC is close to the GPR, which can transport tens of tons of terrestrial sediments down to the deep sea. The average depositional rate can be up to 1 cm per year (Su et al. 2018). The sparker seismic and SBP sections both show sharp and evident seismic truncational structures at the seafloor, across or along the Xiaoliuchiu channel (Figs. 3, 4, 5, and 6), which indicate active seafloor erosion. In addition, a sub-bottom profile (Fig. 4) suggests a NW–SE-trending down-lap feature sub-merging to a flat surface. This indicates that the present-day flow direction is from the GPC to the Xiaoliuchiu platform, which is consistent with the bottom current direction indicated by the ADCP current field (Figs. 1 and 3). Furthermore, a sparker seismic profile shows only less than 1 km northwestward shift of the GPC thalweg, which suggests that the GPC is relatively stable and migrates only slightly (Fig. 3). The sparker seismic and sub-bottom profiles both show active erosional channels gathered in the mouth of the GPR and adjacent to the Xiaoliuchiu islet. There are no clues about the existence of a paleo GPC or its tributaries. Thus, it is suggested that the Xiaoliuchiu channel is probably an active erosional channel in the uppermost GPC area.

Erosion rate estimation in the Xiaoliuchiu channel

The Xiaoliuchiu channel is located north of the Xiaoliuchiu islet (Fig. 1b); it is a NW–SE trending depression which is, on an average, 40 m lower than the west bank of the GPC. The seismic data interpretations from this study suggest that an intense seafloor erosion digs down the TST sequence, exposing it on the seafloor. Before estimating the erosion rate, the seismic sequence identification and corresponding age control need to be examined. In the absence of sediment core data, global sea-level variations are used in order to provide age constraints for the interpreted seismic sequences. Lambeck et al. (2014) collected relative sea level data from globally available sediment samples and atolls along the Pacific and Indian Ocean coasts. They further performed an inversion to estimate global sea level variations in the past 35 ka by considering the average ice volume melting that causes a lithospheric response (i.e., isostatic approach). Their results show that the LGM period started 30 ka before present, when the sea level dropped to 121 m below the present-day sea surface. Between 29 and 21 ka, the sea level gradually fell to from 134 m, attaining the maximum sea level drop, to rising again to 120 m at 16.5 ka. The deglacial period is between 16.5 and 8.2 ka. In Fig. 2, the SB interface is the sequence boundary indicating the last sea-level drop, which is 137.5 m in the Xiaoliuchiu channel (i.e., position 12–13 km in Fig. 3) below the present-day sea level, indicated by the average paleo-seafloor depth, and is very close to that mentioned in Lambeck et al. (2014). This indicates that our seismic

sequence identification is reliable. The 137.5-m depth is slightly lower than 134.5 m, which is probably due to discrepancies in the application of water P wave velocity to estimate true sequence depth. Furthermore, our study area is located in a region of active collision, where tectonic uplift and erosion rate can also affect paleo-seafloor depth estimation. Thus, the age model of Lambeck et al. (2014) could be adopted to correlate the results to seismic para-sequence interpretations in first order, which are LST between 30 and 16.5 ka; TST between 16.5 and 8.2 ka; and HST deposited after 8.2 ka. At seismic section position 11.7 km of Fig. 3, the top of the TST (i.e., MFS) merges with the seafloor, which indicates that the overriding HST no longer exists. In addition, concerning outside of Xiaoliuchiu channel (i.e. relative non erosional area), HST thickness in east bank of the GPC (i.e. position 5-9 km in Fig. 6) is about 50 meters thick which is similar with west bank of the GPC (i.e., position 0-2 km in Fig. 3). Besides, previous studies also pointed out most of turbidity sediments induced at GR mouth moves along the GPC directly and sediments from suspension flow sprayed out at river mouth then deposited on both banks of the GPC (Liu et al. 2016; Su et al. 2018). This leads to a relative stable depositional environment on both banks of the uppermost GPC. Therefore, assuming that the HST thickness was more or less the same on both banks of the GPC before seafloor erosion, minimum 50-m thick HST disappeared on the middle of Xiaoliuchiu channel, east bank of the GPC. Thus, the average erosion rate can be estimated as 609 cm/ka in the middle of the Xiaoliuchiu channel, east bank of the GPC. Furthermore, if whole sequences from the paleo-seafloor (interface SB in Fig. 3) to the present-day seafloor are considered, sediments of approximately 87-m thickness were lost since 35 ka, and the average erosion rate is 248.6 cm/ka. The erosion rate in between 8.2 ka (i.e., HST) and present-day is almost twice that of 35 ka and present-day. According to Lambeck et al. (2014), the sea level was 20 m below the present-day sea surface at 8.2 ka. If the seismic sequence prior to erosion is traced back, the sea level above the mud diapir is approximately 22 m (dashed line in Fig. 3); therefore, it is reasonable to infer that mud diapir activity caused seafloor erosion in the past 8.2-ka period.

Seafloor obstacle and bottom current erosion

Previous studies show that variations in wind or physical properties of water column could induce bottom currents and can cause seafloor erosion (Stow et al. 2018). By definition, the bottom current typically flows along a high topographic gradient (e.g., continental slope and deep-sea basin transition) and develops the supposed contour current. The magnitude of the contour current may increase up to tens of centimeters per second (Hernandez-Molina et al. 2008). Thus, the contour current may sculpt the seafloor and form erosional features, such as furrow or moat (Chen et al. 2019). In

addition, seafloor obstacles, such as the seamount or ridge, could block the bottom current and create a circular erosional feature. Nevertheless, once the bottom current intrudes a narrow topographic area (i.e., channel), it accelerates the current along the depth (topographic narrowing effect; Jan et al. 2002) and enhances seafloor erosion (Gasser et al. 2017). When the current speed exceeds 80 cm/s, carrying with it coarse seafloor sediments (i.e., silt or sand), the bottom current is capable of eroding the seafloor (Hjulstrom 1935). The concept of bottom current can also be applied to shallow water areas (Hernandez-Molina et al. 2008). For example, the Brazilian current accelerates bottom current up to 1.2 m/s and erodes the shelf break area, forming shelf-edge escarpment, erosional terraces, and furrows (Viana et al. 1998a, b, 2002a, b; Viana 2001). Gasser et al. (2017) indicated that the Mediterranean outflow water interacts with the seafloor and causes plenty of erosive channels and furrows when traversing the narrow Strait of Gibraltar. Jan et al. (2002) suggested that the Kuroshio branch current flows through the topographic narrow zone, Penghu channel, and amplifies the bottom current speed, causing corresponding seafloor erosion. The current keeps heading north and is blocked by the Chang-Yu basement high and erodes the seafloor. In our study area, the Xiaoliuchiu islet sits close to the Gaoping shelf break (Fig. 1b), which may block NW–SE trending near-bottom flow induced by the Kuroshio loop current. The bottom current along the Gaoping slope (> 50 m water depth) can split into two branches. The north branch of the bottom current flows clockwise surrounding the islet and then converges with the bottom current in the shelf, amplifying the current (up to 1.5 m/s) and eroding the seafloor. The eroded sediments were probably transported and deposited along the Gaoping slope on the east bank of the GPC (Fig. 7). The southern branch can also erode the seafloor;

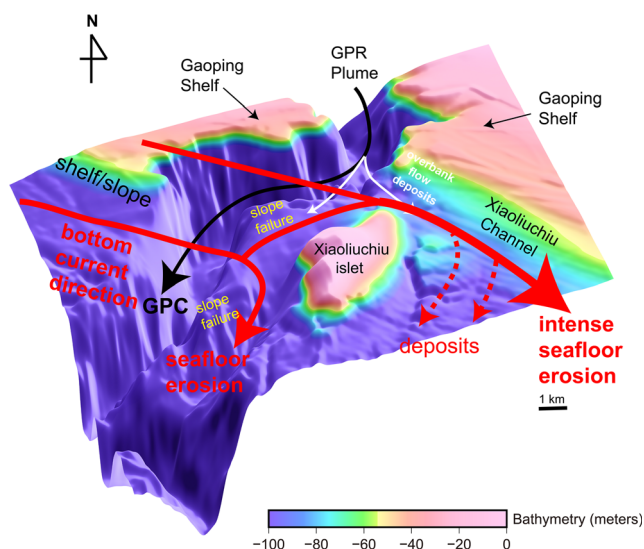


Fig. 7 Sediment transportation model in the uppermost GPC adjacent to Xiaoliuchiu channel. Noted that Xiaoliuchiu islet is suffered by bottom current erosion and mud diapir induced seafloor failure

the bottom current induced by the KC looping also interacted with the mud diapir uplift in the past 8.2 ka, causing slope failure and intense erosion surrounding the Xiaoliuchiu islets. The sediments generated by the slope failure and part of the eroded sediments were transported along the GPC. This probably caused turbidity currents down to the deep sea, and it is possible that one of the turbidity currents is responsible for breaking the telecommunication cable (e.g., Carter et al. 2012; Hsu et al. 2008). Another part of the eroded sediments probably moved across the Gaoping slope on the east bank of the GPC. Notably, continuous and intense bottom current erosion that occurs around the Xiaoliuchiu channel reshaped the Gaoping shelf/slope topography and probably shrank Xiaoliuchiu islet.

Conclusion

The Gaoping Submarine Canyon (GPC) transports a quarter of the terrestrial sediments eroded per year in Taiwan down to the northern South China Sea. Seismic sedimentary structures near the seafloor have been less discussed in the upper reach of the GPC. In this study, a high-resolution marine sparker seismic method was applied to map fine scale sedimentary parasequence structures since the last glacial period. Three major seismic parasequences, namely the lowstand system tract (LST), transgressive system tract (TST), and highstand system tract (HST), were first identified on both banks of the upper reach of the GPC. In contrast to the western bank, only thin TST remained in the north of the Xiaoliuchiu islet, which is probably due to intense seafloor erosion. The integrated data from a deep-towed SBP and ship board ADCP were analyzed; the results suggest that the suspended sediments in the GPR overflowed the GPC at the breakage in the north of Xiaoliuchiu islets. The bottom current induced by the clockwise looping of the annual Kuroshio Current flows along the Gaoping shelf/slope transition and hits the Xiaoliuchiu islet, splitting into two branches. The northern branch amplifies the magnitude of the NW–SE trending bottom current and cuts off the uplifting mud diapir, causing a loss of TST and HST sediments of up to 78-m thickness. The interaction between the bottom current and the mud diapir results in slope failure and a high erosion rate of 609 cm/ka from 8.2 ka, on the east bank of the GPC. The slope failure may be one of the causes for the turbidity current in the upper reach of the GPC. It is probable that the eroded sediments in the Xiaoliuchiu channel moved across the Gaoping Slope on the east bank of the GPC.

Supplementary Information The online version contains supplementary material available at <https://doi.org/10.1007/s00367-020-00673-5>.

Acknowledgments We are grateful for the crew of *R/V Ocean Research I* (ORI-1179 and ORI-1180 cruises) and *R/V Ocean Research III* (ORIII-2019 cruise) for helping us to collect precious geophysical data. Special thanks belong to Mr. Shye-Dong Chiu and Mr. Hsin-Sung Hsieh for

helpful discussions on deployment techniques during high-resolution marine geophysical surveys. Mr. Jay Li from the Department of Oceanography, National Sun-yat sen University, provided thoughtful comments on the dynamics of ocean currents. The constructive comments from Joonas Virtasalo and an anonymous reviewers helped to revise this paper that is appreciated very much.

References

- Carter L, Milliman JD, Talling PJ, Gavey R, Wynn RB (2012) Near synchronous and delayed initiation of long run-out submarine sediment flows from a record-breaking river flood, offshore Taiwan. *Geophys Res Lett* 39:L12603. <https://doi.org/10.1029/2012GL051172>
- Chen SC, Hsu SK, Wang Y, Chung SH, Chen PC, Tsai CH, Liu CS, Lin HS, Lee YW (2014) Distribution and characters of the mud diapirs and mud volcanoes off southwest Taiwan. *J Asian Earth Sci* 92:201–214. <https://doi.org/10.1016/j.jseae.2013.10.009>
- Chen SC, Tsai CH, Hsu SK, Yeh YC, Liu CS, Chung SH, Wei CY (2018) Fangliao Slide—a large slope failure in the upper Kaoping Slope off southwest Taiwan. *Terr Atmos Ocean Sci* 29:17–30. <https://doi.org/10.3319/TAO.2017.06.14.01>
- Chen H, Zhang W, Xie X, Ren J (2019) Sediment dynamics driven by contour currents and mesoscale eddies along continental slope: a case study of the northern South China Sea. *Mar Geol* 409:48–66. <https://doi.org/10.1016/j.margeo.2018.12.012>
- Chiang CS, Yu HS (2006) Morphotectonics and incision of the Kaoping submarine canyon, SW Taiwan orogenic wedge. *Geomorphology* 80(3–4):199–213. <https://doi.org/10.1016/j.geomorph.2006.02.008>
- Chiang CS, Yu HS (2008) Evidence of hyperpycnal flows at the head of the meandering Kaoping Canyon off SW Taiwan. *Geo-Marine Letters* 28(3):161–169. <https://doi.org/10.1007/s00367-007-0098-7>
- Chiang CS, Yu HS (2011) Sedimentary erosive processes and sediment dispersal in Kaoping submarine canyon. *Science China Earth Sciences* 54(2):259–271. <https://doi.org/10.1007/s11430-010-4076-y>
- Chiang CS, Hsiung KH, Yu YS, Chen SC (2020) Three types of modern submarine canyons on the tectonically active continental margin offshore southwestern Taiwan. *Mar Geophys Res* 41(4). <https://doi.org/10.1007/s11001-020-09403-z>
- Dadson SJ, Hovius N, Chen H, Dade WG, Hsieh ML, Willett SD, Hu JC, Horng MJ, Chen MC, Star CP, Lague D, Lin JC (2003) Links between erosion, runoff variability and seismicity in the Taiwan orogeny. *Nature* 426:648–651. <https://doi.org/10.1038/nature02150>
- Gasser M, Pelegri JL, Emelianov M, Bruno M, Gracia EG, Pastor M, Peters H, Rodriguez-Santana A, Salvador J, Sanchez-Leal RF (2017) Tracking the Mediterranean outflow in the Gulf of Cadiz. *Prog In Ocean* 157:47–71. <https://doi.org/10.1016/j.pocan.2017.05.015>
- Harris PT, Whiteway T (2011) Global distribution of large submarine canyons: Geomorphic differences between active and passive continental margins. *Marine Geology* 285:69–86. <https://doi.org/10.1016/j.margeo.2011.05.008>
- Hernandez-Molina FJ, Liave E, Stow DAV (2008) Chapter 19 Continental Slope Contourites. *Developments in Sedimentology* 60:379–408. [https://doi.org/10.1016/S0070-4571\(08\)10019-X](https://doi.org/10.1016/S0070-4571(08)10019-X)
- Hjulstrom F (1935) Studies of morphological activity of rivers as illustrated by the River Fyris. *Bulletin of the Geological Institute University of Uppsala* 25:221–227
- Hsiung KH, Yu HS, Chiang CS (2018) The modern Kaoping transient fan offshore SW Taiwan: morphotectonics and development. *Geomorphology* 300:151–163. <https://doi.org/10.1016/j.geomorph.2017.10.013>
- Hsu SK, Kao J, Lo CL, Tsai CH, Doo WB, Ku CY, Sibuet JC (2008) Turbidity currents, submarine landslides and the 2006 Pingtung Earthquake off SW Taiwan. *Terr Atmos Ocean Sci* 19(6):767–772. [https://doi.org/10.3319/TAO.2008.19.6.767\(PT\)](https://doi.org/10.3319/TAO.2008.19.6.767(PT))
- Hsu SK, Lin SH, Wang SY, Tsai CH, Doo WB, Chen CS, Lin JY, Yeh YC, Wang HF, Su CW (2018) Seabed gas emissions and submarine land-slides off SW Taiwan. *Terr Atmos Ocean Sci* 29:7–15. <https://doi.org/10.3319/TAO.2016.10.04.01>
- Jan S, Wang J, Chern C-S, Chao S-Y (2002) Seasonal variation of the circulation in the Taiwan Strait. *J Mar Sys* 35:249–268. [https://doi.org/10.1016/S0924-7963\(02\)00130-6](https://doi.org/10.1016/S0924-7963(02)00130-6)
- Jan S, Tseng YH, Dietrich DE (2010) Sources of water in the Taiwan Strait. *J Ocean* 66:211–221. <https://doi.org/10.1007/s10872-010-0019-7>
- Jan S, Wang SH, Yang KC, Yang YJ, Chang MH (2019) Glider observations of interleaving layers beneath the Kuroshio primary velocity core east of Taiwan and analyses of underlying dynamics. *Sci Rep* 9:11401. <https://doi.org/10.1038/s41598-019-47912-z>
- Lacombe O, Angelier J, Mouthereau F, Chu HT, Deffontaines B, Lee JC, Rocher M, Chen RF, Siame L (2004) The Liuchiu Hsu island offshore SW Taiwan: tectonic versus diapiric anticline development and comparisons with onshore structures. *Comptes Rendus Geoscience* 336:815–825. <https://doi.org/10.1016/j.crte.2004.02.007>
- Lambeck K, Rouby H, Purcell A, Sun Y, Sambridge M (2014) Sea level and global ice volumes from the Last Glacial Maximum to the Holocene. *PNAS* 111:43: 15296–L. <https://doi.org/10.1073/pnas.1411762111>
- Le Bot P, Kermabon C, Lherminier P, Gaillard F (2011) CASCADE V6.1: Logiciel de validation et de visualisation des mesures ADCP de coque. Rapport technique OPS/LPO 11-01, IFREMER, Centre de Brest, France.
- Levchenko OV, Roslyakov AG (2010) Cyclic sediment waves on western slope of the Caspian Sea as possible indicators of main transgressive/regressive events. *Quaternary International* 225:210–220. <https://doi.org/10.1016/j.quaint.2009.12.001>
- Liu CS, Huang IL, Teng LS (1997) Structural features off southwestern Taiwan. *Mar Geol* 137:305–319. [https://doi.org/10.1016/S0025-3227\(96\)00093-X](https://doi.org/10.1016/S0025-3227(96)00093-X)
- Liu CS, Liu SY, Lallemand SE, Lundberg N, Reed D (1998) Digital elevation model offshore Taiwan and its tectonic implications. *Terr Atmos Oceans Sci* 9(4): 705–738. 10.0.12.247/TAO.1998.9.4.705(TAICRUST)
- Liu JT, Hsu RT, Hung JJ, Kao SJ, Chang YP, Huh CA, Wang YH, Lee CL, Yang RJ (2016) From the highest to the deepest: the Gaoping River-Gaoping Submarine Canyon dispersal system. *Earth-Science Reviews* 153:274–300. <https://doi.org/10.1016/j.earscirev.2015.10.012>
- Mitchum RM, Vali PR, Sangree JB (1977) Seismic stratigraphy and global changes of sea level: Part 6: Stratigraphic interpretation of seismic reflection patterns in depositional sequences: Section 2. Application of seismic reflection configuration to stratigraphic interpretation in C. E. Payton, ed. *Seismic stratigraphy- applications to hydrocarbon exploration: AAPG Memoir* 26:117–133. <https://doi.org/10.1306/M26490C8>
- Nan F, Xue H, Yu F (2015) Kuroshio intrusion into the South China Sea: a review. *Progress in Oceanography* 137:314–333. <https://doi.org/10.1016/j.pocan.2014.05.012>
- Stockwell JW, Cohen JK (2002) The new SU user's manual. Golden: CWP, Colorado School of Mines. <https://doi.org/10.1007/BFb0012094>
- Stow D, Smillie Z, Esentia IP (2018) Deep-sea bottom current: their nature and distribution. In *Encyclopedia of ocean sciences: earth systems and environmental sciences* (3 ed.).
- Su CC, Hsu ST, Hsu HH, Lin JY, Dong JJ (2018) Sedimentological characteristics and seafloor failure offshore SW Taiwan. *Terr*

- Atmos Ocean Sci 29(1):65–76. <https://doi.org/10.3319/TAO.2017.06.21.01>
- Sun CC, Liu CS (1993) Mud dipir and submarine channel deposits in offshore Kaohsiung-Hengchun, southwest Taiwan. *Petroleum Geology of Taiwan* 28:1–14
- Vail PR, Mitchum Jr RM, Thompson III S (1977) Seismic stratigraphy and global changes of sea level: Part 3. Relative changes of sea level from costal onlap: Section 2. Application of seismic reflection configuration to stratigraphic interpretation In: *Seismic stratigraphy—applications to hydrocarbon exploration*, 1st edn. American Association of Petroleum Geologists, pp 63–81.
- Van Wagoner JC, Posamentier H, Mitchum RM, Vail PR, Sarg JF, Loutit TS, Hardenbol J (1988) An overview of the fundamentals of sequence stratigraphy and key definitions. *Soc. Econ. Paleontol Mineral Spec Publ* 42:39–46
- Van Wagoner JC, Mitchum JC, Campion K, Rahmanian V (1990) Siliciclastic sequence stratigraphy in well logs, cores, and outcrops: concepts for high-resolution correlation of time and facies. *The American Association of Petroleum* 7:55. <https://doi.org/10.1306/Mth7510>
- Viana AR (2001) Seismic expression of shallow- to deep-water contourites along the south-eastern Brazilian margin. *Mar Geophys Res* 22:509–521. <https://doi.org/10.1023/A:1016307918182>
- Viana AR, Faugères JC, Stow DAV (1998a) Bottom-current controlled sand deposits: a review from modern shallow to deep water environments. *Sediment Geol* 115:53–80. [https://doi.org/10.1016/S0037-0738\(97\)00087-0](https://doi.org/10.1016/S0037-0738(97)00087-0)
- Viana AR, Faugères JC, Kowsman RO, Lima JAM, Caddah LFG, Rizzo JG (1998b) Hydrology, morphology and sedimentology of the Campos continental margin, offshore Brazil. *Sediment Geol* 115:133–158. [https://doi.org/10.1016/S0037-0738\(97\)00090-0](https://doi.org/10.1016/S0037-0738(97)00090-0)
- Viana AR, De Almeida W, De Almeida CW (2002a) Upper slope sands: Late Quaternary shallow-water sandy contourites of Campos Basin, SW Atlantic margin. *Geol Soc London Mem* 22:261–270. <https://doi.org/10.1144/GSL.MEM.2002.022.01.19>
- Viana AR, Hercos C, De Almeida W, Magelhaes JL, De Andrade SB (2002b) Evidence of bottom current influence on the Neogene to Quaternary sedimentation along the northern Campos slope, SW Atlantic margin. *Geol Soc London Mem* 22:249–260. <https://doi.org/10.1144/GSL.MEM.2002.022.01.18>
- Wessel P, Smith WHF, Scharroo R, Luis JF, Wobbe F (2013) Generic mapping tools: improved version released. *EOS Trans AGU* 94:409–410. <https://doi.org/10.1002/2013EO450001>
- Yang Q, Liu H, Lin P (2020) The effect of oceanic mesoscale eddies on the looping path of the Kuroshio intrusion in the Luzon Strait. *Sci Rep* 10:636. <https://doi.org/10.1038/s41598-020-57487-9>
- Yu HS, Auster PJ, Cooper RA (1993) Surface geology and biology at the head of Kaoping canyon off southwestern Taiwan. *Terr Atmos Ocean Sci* 4(4):441–455
- Yu HS, Chiang CS, Shen CM (2009) Tectonically active sediment dispersal system in SW Taiwan margin with emphasis on the Gaoping (Kaoping) Submarine Canyon. *J Mar Syst* 76(4):369–382. [https://doi.org/10.3319/TAO.1993.4.4.441\(O\)](https://doi.org/10.3319/TAO.1993.4.4.441(O))
- Yu SW, Tsai LL, Talling PJ, Lin AT, Mii HS, Chung SH, Horng CS (2017) Sea level and climatic controls on turbidite occurrence for the past 26 kyr on the bank of the Gaoping Canyon off SW Taiwan. *Mar Geol* 392:140–150. <https://doi.org/10.1016/j.margeo.2017.08.011>

Publisher's note Springer Nature remains neutral with regard to jurisdictional claims in published maps and institutional affiliations.